

Global test of modified precompound decay models

M. Blann and H. K. Vonach*

E-Division, Lawrence Livermore National Laboratory, Livermore, California 94550

(Received 18 February 1983)

A single parameter set was adopted for the hybrid and geometry dependent hybrid models. The nuclear density profile was modified for consistency with results of the Myers nuclear droplet model. Optical model parameters were modified to give better global results for inverse reaction cross sections in the precompound energy range up to 90 MeV. Two types of multiple precompound decay processes are defined, and the more important of the two is incorporated into the precompound decay formalism. This results in two to five orders of magnitude improvement in predicting $^{202}\text{Hg}(p,2p)$ and $^{202}\text{Hg}(p,2pn)$ product yields for proton energies up to 86 MeV. The global parameter set and formulation of this work is compared with (n,xn) and (n,p) spectra for 14 MeV incident neutrons, for (p,n) spectra with 18–90 MeV protons, and with (p,p') spectra for 39–90 MeV protons. The geometry dependent hybrid model gives the better overall agreement, in most cases within the 20–30% limit of significance attached to the model. Some discussion is given of methods by which the calculations might be further improved.

NUCLEAR REACTIONS Hybrid, geometry dependent hybrid precompound decay models, improve global parameter set, implement multiple precompound decay. Test new formulation vs spectra from reactions induced by 14 MeV neutrons to 90 MeV protons.

I. INTRODUCTION

The exciton model of Griffin provided the first explanation of the spectral shapes of nucleons emitted with continuous spectra for energies in excess of those characteristic of equilibrium evaporation.^{1–4} Several years after the exciton model was proposed, its basic premise was extended to permit *a priori* prediction of the magnitudes as well as spectral shapes of these “precompound” or “preequilibrium” particles.^{5–19}

These relatively simple, closed form precompound decay models have been surprisingly successful in reproducing a large body of experimental data.¹⁹ Among these models the hybrid⁶ and geometry dependent hybrid (GDH) models⁷ have been reasonably successful in reproducing a broad range of data in an *a priori* mode.⁹ This was accomplished with several choices of parameter options, giving rather similar results.

The data set currently available covers a much broader range than that in existence when the earlier work was done. The question is how well these models fare when confronted with a more extensive set of data. Perhaps it is more valuable to ask the question of how well the models will do if restricted to a single choice of parameters for all projectile energies, and the reactions of the types (n,n'), (p,p'), (n,p), and (p,n). If such comparisons give good results, then discrepancies between calculation and data may give insights into physical aspects of the individual reactions, e.g., microscopic influences on the intranuclear nucleon-nucleon scattering processes.

In this work we have used a part of the currently available data as an aid in selecting a single mode of calculation

for the hybrid and GDH models, in order to see how well a single parameter set will globally reproduce these data. In so doing, minor *ad hoc* (but physically reasonable) adjustments have been made of a few model parameters. An important modification has been made to account for one type of multiple precompound decay, which was excluded in earlier hybrid model formulations, and which becomes significant at the higher excitation energies to be considered in this work. The single parameter set to be used is not unique, as will be discussed. Rather the values are one of many mutually consistent sets. This set, which will be described in Sec. II, will be used to generate calculated results for comparison with data in Sec. III. This parameter set has been entered into the revised ALICE code^{20,21} (ALICE/LIVERMORE 82) (Ref. 22) as a default set for nucleon induced reactions, relieving users of this code of the requirement of selecting between the many possible precompound options (some combinations of which are not mutually consistent). Emphasis will be placed on the GDH model, for it provides a potentially better description of the physical process, i.e., a higher probability of peripheral collisions to undergo precompound decay than for central collisions. This can be an important point if the precompound calculation is to be followed by a fission calculation, for which the fission barrier is expected to be angular momentum dependent. In such a case preferential precompound depletion of higher partial waves can be an important factor to consider. Possible future inclusion of neutron skin effects in the precompound description would also favor the additional detail offered by the GDH option.

In Sec. II we review the hybrid and GDH formulations,

TABLE I. Definition of symbols.

$P_\nu(\epsilon)d\epsilon$	Number of particles of the type ν (neutrons or protons) emitted into the unbound continuum with channel energy between ϵ and $\epsilon+d\epsilon$ (MeV)
$P_\nu(l,\epsilon)d\epsilon$	As for $P_\nu(\epsilon)$, but evaluated for the l th partial wave
\bar{n}	Equilibrium (most probable) particle plus hole (exciton) number
n_0	Initial exciton number
${}_nX_\nu$	Number of particles of type ν (proton or neutron) in an n exciton hierarchy
E	Composite system excitation
U	Residual nucleus excitation
$N_n(\epsilon,U)$	Number of ways that n excitons may be combined such that one, if emitted, would have channel energy ϵ and the remaining $n-1$ excitons would share excitation $U=E-B_\nu-\epsilon$, where B_ν is the particle binding energy
$N_n(E)$	Number of combinations with which n excitons may share excitation energy E
$\lambda_c(\epsilon)$	Emission rate of a particle into the continuum with channel energy ϵ
$\lambda_+(\epsilon)$	Intranuclear transition rate of a particle which would have channel energy ϵ if it were emitted into the continuum
D_n	Fraction of the initial population which has survived to an n -exciton hierarchy
σ_R	Reaction cross section
l	Orbital angular momentum in units \hbar
T_l	Transmission coefficient for l th partial wave
$d(R_l)$	Nuclear density at radius R_l , where l denotes the entrance channel orbital angular momentum
d_s	Saturation density of nuclear matter
λ	Reduced de Broglie wavelength
σ_l	Partial reaction cross section for the incident l th partial wave
g_ν	Single particle level density for particle type ν
N	Target neutron number
Z	Target proton number
ϵ_f	Fermi energy
B_ν	Binding energy of particle type ν
ϵ	Channel energy
C_n	Cross section for emitting one and only one neutron summed over exciton number
C_p	As for C_n , but proton only cross section.
C_{np}	Cross section summed over exciton number for which one neutron and one proton are estimated to have been emitted from a single nucleus in the same exciton number configuration
$C_{nn} (C_{pp})$	Cross section summed over exciton number for which it is estimated that two neutrons (protons) are emitted from the same nucleus and exciton number

with attention to the modifications and extensions of the model. We discuss the uncertainties in the parameters entering the use of the model and test the assumptions made in extending the model to include multiple precompound emission. In Sec. III the new formulation with a single parameter set is confronted with a broad range of particle spectral data for nucleon induced reactions. These

results are discussed in Sec. III, and the conclusions of this work are summarized in Sec. IV.

II. FORMULATION AND MODIFICATIONS

A. General description

The hybrid model for precompound decay is formulated as

$$P_\nu(\epsilon)d\epsilon = \sum_{\substack{n=n_0 \\ \Delta n = +2}}^{\bar{n}} [X_n X_\nu N_n(\epsilon, U)/N_n(E)] g d\epsilon \\ \times [\lambda_c(\epsilon)/(\lambda_c(\epsilon) + \lambda_+(\epsilon))] D_n \quad (1)$$

and

$$\frac{d\sigma_\nu(\epsilon)}{d\epsilon} = \sigma_R P_\nu(\epsilon), \quad (2)$$

where the symbols are defined in Table I. The quantity in the first set of square brackets of Eq. (1) represents the number of particles to be found (per MeV) at a given energy ϵ (with respect to the continuum) for all scattering processes leading to an “ n ” exciton configuration. It has been demonstrated that the nucleon-nucleon scattering energy partition function $N_n(E)$ is identical to the exciton state density $\rho_n(E)$, and may be derived when certain conditions on N-N (nucleon-nucleon) scattering cross sections are met.²³ This point is discussed in the Appendix.

The second set of square brackets in Eq. (1) represents the fraction of the ν type particles at energy ϵ which should undergo emission into the continuum, rather than making an intranuclear transition. The D_n represents the average fraction of the initial population surviving to the exciton number being treated. The products involved in Eq. (1) may be seen to be time independent; no Heisenberg principle contradiction is involved.

Early comparisons between experimental results, precompound exciton model calculations, and intranuclear cascade (INC) calculations⁵ indicated that the exciton model gave too few precompound particles and that these were too soft in spectral distribution for the expected initial exciton configurations. The INC results indicated that the exciton model deficiency resulted from a failure to properly reproduce enhanced emission from the nuclear surface.

In order to provide a first order correction for this deficiency the hybrid model was reformulated as a sum of contributions, one term for each entrance channel impact parameter. In this way the diffuse surface properties sampled by the higher impact parameters were crudely incorporated into the precompound decay formalism, in the geometry dependent hybrid model (GDH). The differential emission spectrum is given in the GDH as

$$\frac{d\sigma_\nu(\epsilon)}{d\epsilon} = \pi\lambda^2 \sum_{l=0}^{\infty} (2l+1) T_l P_\nu(l, \epsilon), \quad (3)$$

where the symbols are defined in Table I. Whereas the intranuclear transition rates entering (1) are evaluated for nuclear densities averaged over the entire nucleus, those appropriate to (3) should be averaged over the densities corresponding to the entrance channel trajectories, at least for the contributions from the first projectile-target interaction.

The geometry dependent (surface) influences are manifested in two distinct manners in the formulation of the GDH model. The more obvious is the longer mean free path predicted for nucleons in the diffuse surface region. It has been shown⁷ that this effect changes the predicted

emission cross section about the same as would a factor of 2 increase in the mean free path in the formulation of the hybrid model, Eq. (1). (The evaluation of these parameters will be discussed further on in this section.)

The second effect is less physically secure, yet seems to be important in reproducing experimental spectral shapes. This is the assumption that the hole depth is limited to the value of the Fermi energy which is calculated for each trajectory in a local density approximation. The result of this is to effectively reduce the degrees of freedom, especially for the higher partial waves (for which a lower maximum hole depth is predicted), thereby hardening and enhancing the predicted emission spectra. The separate influences of these two surface (geometric) effects have been illustrated previously.⁷ In this work we assume the restriction on hole depth in the GDH model to be restricted to the first collision, for which there is some knowledge of average density at the collision site.

Following these general comments on the models, we next describe the details of their evaluation, as in previous work, and as modified for the global default parameters to be used in these calculations.

B. Parameter evaluation and modification

1. Nuclear density distribution

The original GDH model, and codes using this model, employed a Fermi density distribution function,

$$d(R_l) = d_s [\exp(R_l - C)/0.55 \text{ fm} + 1]^{-1} \quad (4)$$

with

$$C = 1.07A^{1/3} \text{ fm}, \quad (5)$$

taken from electron scattering results.²⁴ The radius for the l th partial wave was defined by

$$R_l = \lambda(l + \frac{1}{2}). \quad (6)$$

The charge radius C of Eq. (5) has been replaced in the present parametrization by a value characteristic of the matter (rather than charge) radius based on the droplet model work of Myers,²⁵ plus an *ad hoc* projectile range parameter λ ,

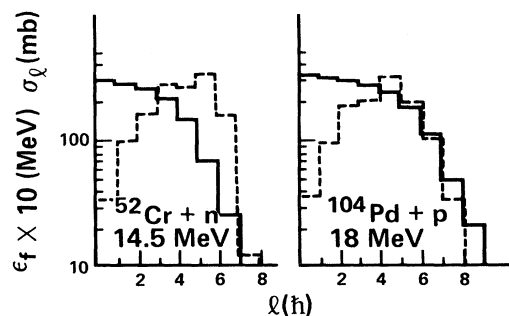


FIG. 1. Fermi energy and partial reaction cross sections versus impact parameter for ^{52}Cr and 14.5 MeV neutrons and for ^{104}Pd + 18 MeV protons. The local density Fermi energies are given by the solid histogram; the partial reaction cross section are given by the dashed histogram.

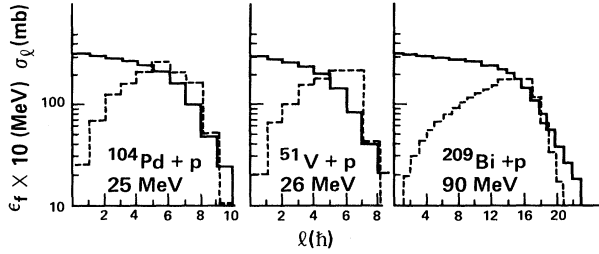


FIG. 2. As in Fig. 1 for $^{104}\text{Pd} + 25$ MeV protons, $^{51}\text{V} + 26$ MeV protons, and $^{209}\text{Bi} + 90$ MeV protons.

$$C = 1.18A^{1/3}[1 - 1/(1.18A^{1/3})^2] + \lambda. \quad (7)$$

The result of using Eq. (7) rather than (5) in evaluating the nuclear density distribution is supported by comparing the optical model T_l results with densities evaluated at R_l defined by Eq. (6) in Eq. (4). With Eq. (7), the T_l go toward zero as the densities at R_l go toward zero. The alignment was much poorer with C evaluated from (5), which caused an unphysical inconsistency in parameters, particularly at lower projectile energies. Examples of σ_l and ϵ_f vs l (which is related to the average density) as computed with Eqs. (4), (6), and (7) are shown in Figs. 1 and 2. These results will be discussed in greater detail in Secs. III and IV.

The earlier result using Eq. (5) led, at lower projectile energies, to the unphysical case of substantial partial reaction cross sections from the optical model routine predicted at radii for which Eq. (4) gave essentially zero density. This may still be a problem at lower projectile energies even with the present parametrization. We believe that the localization implied by the GDH formula should completely disappear at the lower projectile energies. The relationship between σ_l from the optical model codes and the density from Eqs. (4) and (7) determines the degree to which this is so, in context of results of the calculations.

In the hybrid model the average nuclear density is calculated by integration and averaging of (4) between $R = 0$ and $R = C + 2.75$ fm. Details of the integration have been given previously.⁹ The Fermi energy (ϵ_f) has been taken as 40 MeV for saturation density, and is assumed to vary as the average density to the two-thirds power. The value of ϵ_f so evaluated is used in defining the single particle level density “ g ” for all calculations, hybrid and GDH, as this should be a property of the average potential.²⁶ The single particle level densities have been defined in the present work by

$$g_n = \frac{N}{20} \left(\frac{\epsilon_f + B_n + \epsilon}{\epsilon_f} \right)^{1/2}, \quad (8a)$$

$$g_p = \frac{Z}{20} \left(\frac{\epsilon_f + B_p + \epsilon}{\epsilon_f} \right)^{1/2}. \quad (8b)$$

In earlier results^{9,18,19} the constant 14 replaced the constant 20 of Eqs. (8). Values of $g_n = N/14$ and $g_p = Z/14$ give nearly identical calculated spectra when used in place of the energy dependent values defined by Eqs. (8).

In the hybrid model, when Pauli corrected nucleon-

nucleon scattering cross sections are used to evaluate the $\lambda_+(\epsilon)$ of Eq. (1), the average value of the Fermi energy (usually ≈ 30 MeV) and density is used to define the nucleon mean free path (mfp). In the geometry dependent hybrid model the Fermi energies and nuclear densities are defined according to impact parameter via Eq. (6). Options have been employed using either the maximum density along each trajectory, or an average. We select the use of the density average in this work and as the code default option. All relevant equations for the averaging process are given elsewhere,⁹ and are used without change. The ϵ_f values determined by the averaged densities also determine the maximum hole depth of the 2p1h and 1p1h configurations of hybrid or GDH calculations, which are used in the $N_n(E)$ functions of Eq. (1) and as discussed in the Appendix.

2. Intranuclear transition rates

The precompound decay models under discussion have employed intranuclear transition rates evaluated both from the imaginary optical potential (using parameters due to Becchetti and Greenlees²⁷) and from Pauli corrected nucleon-nucleon scattering cross sections.²⁸ Both methods gave similar results⁹; however, the optical model parameter set is valid only for projectile energies below 55 MeV. Because we wish to treat data sets considerably in excess of 55 MeV energy, we have adopted the Pauli corrected NN scattering evaluation as the standard default parameter. Recent optical model analyses of proton induced reaction data give mfp results in quite reasonable agreement with the NN scattering results up to around 200 MeV.²⁹

For the reasons discussed above and in Sec. IIA, the Pauli corrected λ_+ values from NN scattering have been used as default parameters for GDH calculations, and the λ_+ are reduced to one-half (mfp is multiplied twofold) when the hybrid model calculation is performed in order to approximate the effects of the diffuse surface. In the default version of GDH, corresponding to results to be presented in Sec. III, we use the option whereby only the first collision is localized according to the impact parameter as implied by Eq. (6), with all higher order precompound terms being treated by the hybrid model—i.e., using nuclear densities averaged over the nucleus and independent of impact parameter. This is reasonable because the excitons can sample nearly the entire nuclear volume after a single scattering, since mfp values are ≈ 4 fm.

3. Initial exciton numbers

The starting point in any nucleon reaction is obviously a 2p1h state. However, the selection of initial n and p particle exciton numbers within this 2p1h state seems to cause the most confusion among users of the precompound routines of the OVERLAD ALICE code. This should be alleviated by internal selection under the default option in the new ALICE/LIVERMORE 82 code. The algorithm coded and used in results to be presented is as follows.

The free scattering n-p cross section σ_{np} is ≈ 3 times the corresponding σ_{nn} or σ_{pp} over the energy range of interest

for the precompound decay calculations under consideration.²⁸ In a nucleon induced reaction there will be a total of two initial particle excitons divided in some averaged manner between neutrons and protons. This should be crudely related to the relative free scattering cross sections, and to the neutron (N) and proton (Z) numbers of the target nucleus.

For an incident neutron, there should therefore be three np pairs for every nn pair if $N=Z$, or five neutron excitons to each three proton excitons, or $\frac{5}{8} \times 2$ neutron excitons and $\frac{3}{8} \times 2$ proton excitons to make the two particle excitons (remembering that we are interested only in the average *particle* exciton numbers, where the projectile is one of the two particle excitons). These results should be weighted further by the numbers of N and Z of the target, giving the default algorithms for neutron induced reactions,

$${}_3X_n = \frac{2(3Z + 2N)}{(3Z + 2N + 3Z)} \quad (9a)$$

and

$${}_3X_p = 2 - {}_3X_n, \quad (9b)$$

and for proton induced reactions

$${}_3X_p = \frac{2(3N + 2Z)}{(3N + 2Z + 3N)} \quad (10a)$$

and

$${}_3X_n = 2 - {}_3X_p. \quad (10b)$$

This is essentially the method used to determine initial exciton numbers in the past, which is now programmed as a default option for nucleon induced reactions. As in the past, the initial X_n and X_p numbers are each assumed to increase by 0.5 in successive values of n in Eq. (1), as the particle exciton number increase is by 1.0.

4. Pairing options

The question of how to introduce pairing into the exciton energy partition functions (exciton state density) of Eq. (1) is, we believe, still open. The most comprehensive experimental program and model analyses on this question are due to Grimes *et al.*³⁰ who measured (p,n) spectra on ¹⁰³Rh, ^{104,105,106,108,110}Pd, and on ^{107,109}Ag at incident proton energies between 18 and 25 MeV. This work made a strong case for reducing the residual excitation for the reactions considered by 2δ , where

$$\delta = 11/A^{1/2}, \quad (11)$$

for all but even-even target nuclei, for which the primary shift was zero following neutron emission, but was expected to be 2δ following proton emission. The end points of the (p,n) data were consistently in agreement with this hypothesis, and we find the same result when refitting the data of Ref. 30. However, the same treatment seems to fail in other cases, so perhaps the question is open. The end point shifts may well be a combination of shell and pairing effects, so that modeling to consider both points may be necessary to global fitting of the last few MeV of

the precompound spectra.

Rather than imposing a pairing treatment, we allow two choices in the new code with the same choice to be used in both precompound and subsequent evaporation calculations. The value of the pairing correction is always defined by Eq. (11), with either a backshift³¹ or standard pairing shift being applied. The standard shift, which will be used in all comparisons in Sec. III, unless noted to the contrary, uses true thermodynamic excitations for odd A nuclei, reduces the excitation by δ for doubly even nuclei, and increases it by δ for doubly odd nuclei. The backshifted option uses true thermodynamic excitation for doubly even nuclei, and increases it by δ for odd A nuclei and 2δ for doubly odd nuclei. The pairing correction influences only the last few MeV of the precompound spectrum to a substantial degree, and we repeat that we feel that the "best" mode of inclusion in precompound decay is still uncertain.

5. Binding energies

The binding energies and Q values used in the present work were all based on experimental masses.³² The ALICE/LIVERMORE 82 code includes experimental masses in block data, so that a simple input parameter results in all Q values and binding energies being internally generated from experimental mass tables.

6. Reaction and inverse reaction cross sections

Comparisons between calculated and experimental spectra are no more meaningful than the uncertainties inherent in each. For example, the scattering distribution functions used in Eq. (1) are shown in the Appendix to have an inherent error in assumptions for their derivation of the order of $\pm 20\%$ at least. Another parameter which must be scrutinized is the value used for the reaction cross section in Eq. (2), and for the inverse reaction cross section for the $\lambda_c(\epsilon)$ in Eq. (1). Comparisons between calculated and experimental spectra cannot be interpreted beyond the "noise level" of these model uncertainties.

The present code has a classical sharp-cutoff routine for inverse reaction cross sections, and the earlier optical model routine. The optical model is the only internal source of entrance channel reaction cross sections for nucleon-induced reactions while either routine may be used for inverse cross sections. In this work the optical model was used for calculating inverse reaction cross sections and composite system reaction cross systems.

The optical model routine in the ALICE code used a pure surface form-factor—parameter set for w for nucleon-induced reactions. While this should be adequate for energies consistent with compound nucleus evaporation, poor results were obtained at the higher energies required (up to 90 MeV) for the precompound studies of interest in the present work. Because we are interested only in generating reaction cross sections and transmission coefficients which are to be used in Eqs. (1)–(3) from these subroutines and not scattering angular distributions, we have made *ad hoc* changes in the optical model parameters in the ALICE/LIVERMORE 82 code, which have been used for

TABLE II. Optical model parameters.

Parameter		Neutrons	Protons
Real potential V (MeV)	48	(Woods-Saxon)	60
Imaginary W (MeV)	9.0		5.0
Form of W	Pure surface		Pure volume
Spin orbit (MeV)	7.0		7.5
Radius			
R_V (fm)	=	$(1.322 - 7.6 \times 10^{-4}A + 4 \times 10^{-6}A^2 - 8 \times 10^{-9}A^3) \times A^{1/3}$	$1.2 \times A^{1/3}$
R_W (fm)	=	$(1.266 - 3.7 \times 10^{-4}A + 2 \times 10^{-6}A^2 - 4 \times 10^{-9}A^3) \times A^{1/3}$	$1.55 \times A^{1/3}$
R_{so} (fm)	=	R_W	$1.25 \times A^{1/3}$
$R_{Coulomb}^{(fm)}$	=	$1.25A^{1/3}$	$1.25 \times A^{1/3}$
Diffusivity			
a_V (fm)	0.66		0.6
a_W	0.48		0.5
a_{so}	0.48		0.51

results presented in this work.

For protons the pure surface absorption used was changed to pure volume absorption. A parameter set given by Perey³³ was used as a starting point and varied arbitrarily to give a reasonable global fit to reaction cross sections between ²⁷Al and ²⁰⁸Pb. The parameter set is summarized in Table II. Results using the parameter set may be seen in Fig. 3. The reaction cross sections are in good agreement with experimental results for all targets to within the $\pm 10\%$ range at $\epsilon_p > 40$ MeV (the points without error bars represent cross sections resulting from

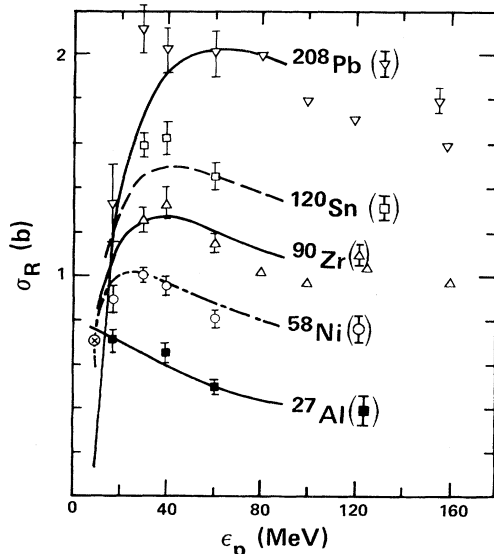


FIG. 3. Experimental and calculated proton reaction cross sections for several targets versus proton energy. The lines give results of the optical model subroutine in the ALICE/LIVERMORE 82 code used in this work. Points give experimental results; see Refs. 33 and 29. The circled \times is a point where all targets shown give nearly the same proton reaction cross section.

a ten parameter optical model search fitting procedure of scattering data²⁹).

At energies near and even somewhat above the Coulomb barrier the global cross sections are in poor agreement with reported experimental results. The calculated low energy cross sections on Sn and Pb seriously underestimate experimental yields, whereas for the Ni targets there is an overestimation of low energy yields. The test of agreement in the near barrier region really rests on very few experimental results. Comparison of calculated and experimental evaporation and precompound spectra in these regions must therefore be interpreted with extreme caution, as the quality of the input (reaction and/or inverse cross sections) may be uncertain.

For neutrons, a parameter set due to Hodgson³⁴ was used as a starting point. The main change was to remove the energy dependence of real and imaginary (pure surface) well depths. The parameter set used is summarized

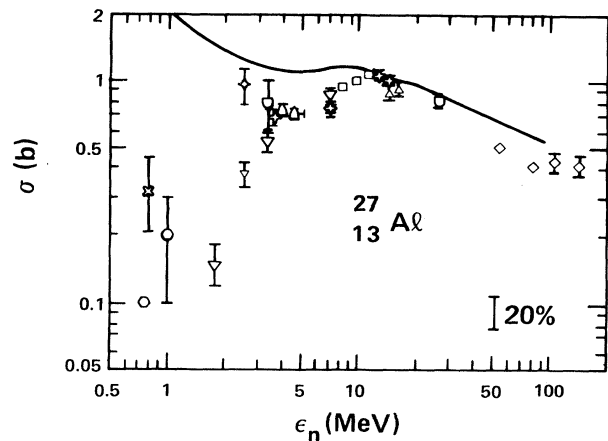


FIG. 4. Total nonelastic cross sections for neutrons on ²⁷Al versus neutron energy. The solid line is the result of the optical model parameter set used in this work, and gives the nonelastic plus compound elastic cross section. References to experimental results are to be found in Ref. 36.

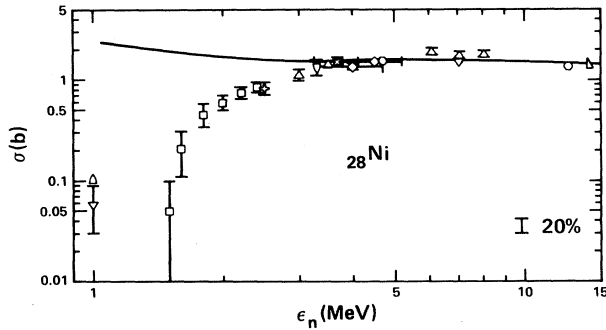


FIG. 5. As in Fig. 4 for a Ni target. See Ref. 36 for sources of experimental cross sections.

in Table II. Comparisons of results with this parameter set with experimental total nonelastic cross sections for ^{27}Al , ^{58}Ni , Sn, and Pb targets are shown in Figs. 4–7.^{35,36} The low energy divergence between theoretical total reaction cross sections and experimental total nonelastic cross sections is vast, and represents the contribution of the compound elastic cross section which is a part of the optical model cross section and not a part of the total nonelastic measurement. In the case of an excited residual nucleus (for which the inverse cross section is properly evaluated) the reduced influence of the Pauli principle should cause the compound elastic cross section to convert to nonelastic channels.²³

While quite satisfactory agreement is shown between the calculated and experimental neutron cross sections for neutron energies above ≈ 10 MeV, the values below ≈ 3 MeV from the optical model subroutine-parameter set of the ALICE and ALICE/LIVERMORE 82 codes are not reliable and are subject to large uncertainties (probably up to 50%). These uncertainties are not important in the precompound decay region, but could be very significant in attempts to fit low energy evaporation neutron spectra and especially in evaluating evaporation-fission competition in fissile nuclides.

The main point of this subsection may be summarized as follows. If one wishes good compound or precompound calculations involving reaction and inverse reaction cross sections in a near barrier region, input must be carefully selected based on experiments on the same (prefer-

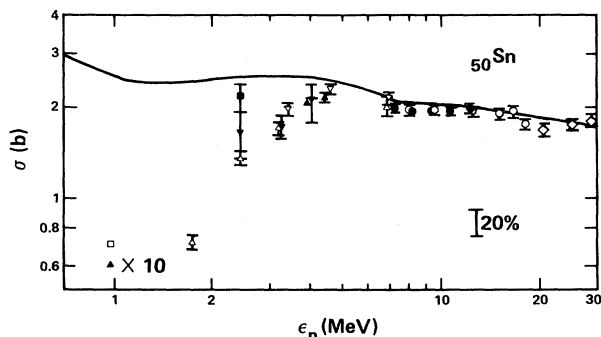


FIG. 6. As in Fig. 4 for a Sn target. See Ref. 35 for sources of experimental cross sections.

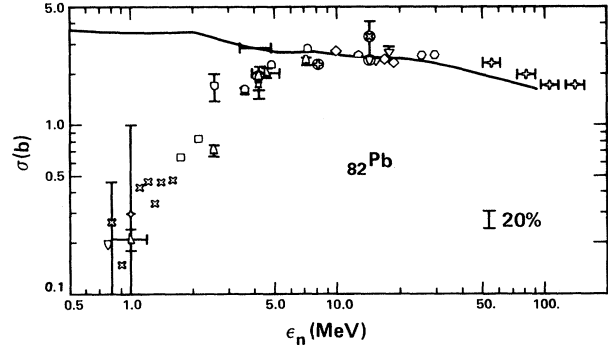


FIG. 7. As in Fig. 4 for a Pb target. See Ref. 36 for sources of experimental cross sections.

ably) or nearly the same target nucleus. Conversely, if a global parameter set (such as the values specified in the ALICE codes) is used in a calculation, extreme care must be exercised before concluding, e.g., that the experimental evaporated protons or α particles are enriched in low kinetic energies over results expected from evaporation theory. This is a simple restatement of the adage that computational output is no better than the input, and points out the difficulties of getting good input in the near barrier region for charged particles, and in the few MeV or lower region for neutrons.

7. Multiple particle emission

Previous hybrid and GDH calculations arbitrarily restricted precompound emission to a total of one particle (neutron plus proton) so that the emission cross section would not exceed the reaction cross section. This should be a good approximation at energies below 50 MeV where Eq. (1) would naturally predict considerably less than one particle emitted by the precompound decay mechanism. However, it becomes increasingly poor as excitation increases.

The multiple precompound decay processes must be considered at higher excitations since they are important in determining the contributions of terms after $n = n_0$ in Eq. (1), in determining the cross section surviving to the (equilibrium) compound nucleus, and in determining yields of products which require multiple precompound emission for population, e.g., a (p,2p) reaction on a heavy element target.

There are two types of multiple precompound decay which might be considered. Type I results when a nucleus emits more than one exciton from a single exciton hierarchy. It may be seen that, e.g., in a two-particle—one-hole configuration, up to two particles could be emitted; in a three-particle—two-hole configuration up to three particles could be emitted, etc. The particle density distribution of these excitons, as given in the first set of brackets in Eq. (1), may be seen to be governed by the total composite system excitation. For illustrative purposes, we show the number of excitons expected at excitations above 8 MeV (taken as an estimate of average particle binding energy) versus composite nucleus excitation in Fig. 8. The importance of considering this “type I” multiple decay mode at

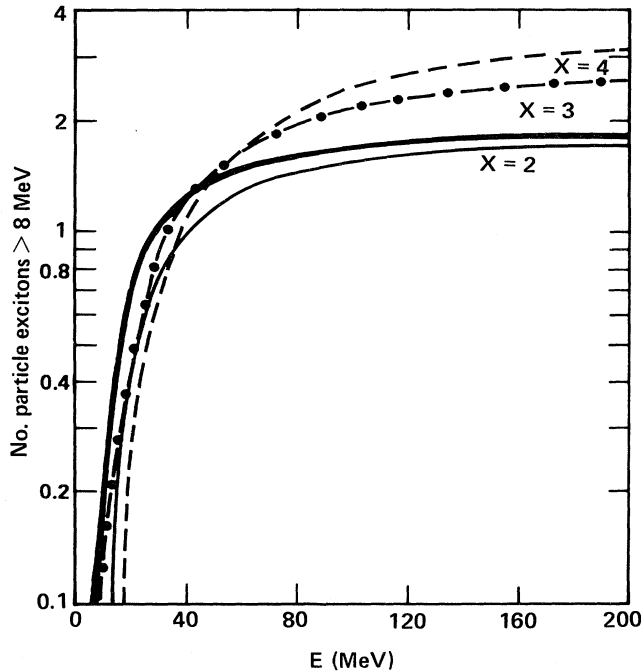


FIG. 8. Number of particle excitons at excitations greater than 8 MeV above the Fermi energy versus composite nucleus excitation and particle excitation number. The heavy solid curve is for a 2p1h configuration, the dotted-dashed curve is for 3p2h, and the dashed curve is for 4p3h. The thin solid curve is for a 2p2h configuration which would be relevant for type II multiple precompound decay as discussed in the text.

excitations above 50 MeV is evident from Fig. 8.

The second type of multiple precompound decay (type II) would be described by the sequence "particle emission, one or more two body intranuclear transitions in daughter nucleus, particle emission." If the intervening two-body transitions are omitted from this sequence, it becomes type I multiple emission.

In the type II sequence for nucleon induced reactions the leading term would be two-particle-two-hole. The particle density for this hierarchy for nucleons above 8 MeV is shown as a function of residual nucleus excitation energy in Fig. 8. It should be recognized that the relevant residual excitation of this population curve should be reduced by the nucleon binding energy and by the kinetic energy of the first emitted nucleon before comparing with the type I curve. Then it may be seen that at excitations below ≈ 50 MeV for the residual nucleus following one particle emission, type II multiple precompound decay should rapidly become small compared with type I decay. We have investigated type II decay quantitatively in work following completion of this paper.³⁷ Results confirm our speculation that type I multiple precompound decay is far more important than type II for the reactions presented in this work.

Because the first particle emission leaves a range of residual excitations and exciton numbers, a calculation of type II emission becomes more complex and time consuming than for type I emission. For this reason we have treated

only type I multiple precompound decay in the present work.

To extend (1) to higher energies and maintain its simplicity, we have made some arbitrary assumptions, as yet untested, to estimate type I multiple particle emission. We next define these assumptions, which are based on simple probability arguments.

If P_n and P_p represent the total numbers of neutron and proton excitons emitted from a particular exciton number configuration, we assume that

$$P_{np} = P_n P_p \quad (12)$$

is the number of either type of particle emitted in coincidence with the other from the same nucleus and exciton hierarchy. This definition covers P_{pn} since in an emission from the same exciton number there is no distinction to be made.

We assume that the number of neutrons which are emitted in coincidence with another neutron from a particular exciton number configuration is given by

$$P_{nn} = 2 \frac{P_n}{2} \frac{P_n}{2} \quad (13)$$

with the fraction of the reaction cross section decaying by the emission of two coincident neutrons being $P_{nn}/2$. The value of P_{nn} is restricted to be $\leq P_n - P_{np}$. Similar expressions are used for proton-proton coincident emissions.

The number of neutrons (protons) emitted from the n -exciton configuration which were not in coincidence with another particle would be given by

$$P_n \text{ (n only)} = P_n - P_{nn} - P_{np} \quad (14a)$$

$$P_p \text{ (p only)} = P_p - P_{pp} - P_{np} \quad (14b)$$

and the fraction of the population F_n which had survived decay of the exciton number in question would be

$$F_n = 1 - P_n \text{ (n only)} - P_p \text{ (p only)} - P_{pp}/2 - P_{nn}/2 - P_{np} \quad (15)$$

This fraction would multiply the fractional population which had survived to the n exciton state, giving the fraction of the original population which is available for decay from the $n+2$ exciton state.

The treatment of multiple emission is completed by storing spectra of excited nuclei into the appropriate daughter nucleus buffers following the emission of one neutron only, one proton only, one neutron and one proton, two neutrons only, and two protons only. The sum of these cross sections plus the cross section predicted to survive to the original parent compound state must equal the reaction cross section. This aspect of the calculation will have very little effect on the predicted emission spectra (none on the precompound spectra) but will have major impact on the predicted excitation functions for products for which one or two neutrons or protons, or one n and one p are emitted in the precompound mode. We describe next the method used for this last step of the precompound calculation, following which the evaporation calculation is performed within the code.

Within each exciton hierarchy we calculate the number of neutrons (protons) emitted in singles, in coincidence with protons, or in coincidence with neutrons as the product of the nucleon numbers from Eqs. (12)–(14) multiplied by the surviving population cross sections and the reaction cross sections. These cross sections [$C_n(C_p)$, C_{np} , C_{nn} , etc.] are defined in Table I.

From the calculated total precompound neutron emission spectrum $d\sigma_n(\epsilon)/d\epsilon$, the cross section which could be involved in the emission of two neutrons is calculated as

$$\sigma_{2n} = \int_{U=0}^{E-B_{2n}} \frac{d\sigma_n(\epsilon)}{d\epsilon} d\epsilon, \quad (16)$$

where B_{2n} represents the sum of first and second neutron binding energies.

Similarly the neutron cross section which could be emitted in coincidence with protons is given by

$$\sigma_{np} = \int_{U=0}^{E-B_n-B_p} \frac{d\sigma_n(\epsilon)}{d\epsilon} d\epsilon, \quad (17)$$

where B_n is the first neutron out binding energy and B_p is the proton binding energy of the daughter nucleus following neutron emission. Similar integrals are made for the proton emission cross section which could consist of two coincident protons, σ_{pp} , and of a proton in coincidence with a neutron σ_{pn} . The cross section available for the emission of a single nucleon $\sigma_{n(p)}$ is of course the sum of all $d\sigma(\epsilon)/d\epsilon$ (the integrals are replaced by sums since the code computes spectra at 1 MeV intervals).

For the daughter nucleus following emission of one and only one precompound neutron, we store

$$\sigma^{A-1,Z}(U) = \frac{d\sigma_n(\epsilon)}{d\epsilon} \frac{C_n}{\sigma_n}, \quad (18)$$

where $U = E - B_n - \epsilon$; for the daughter nucleus following the coincident emission of two neutrons, we store

$$\sigma^{A-2,Z}(U) = \frac{d\sigma_n(\epsilon)}{d\epsilon} \frac{C_{nn/2}}{\sigma_{nn}}, \quad (19)$$

where

$$U = E - B_{2n} - \epsilon - \bar{\epsilon}_n,$$

where $\bar{\epsilon}_n$ is the average kinetic energy of the second neutron for a given energy ϵ of the first neutron. For the case of the daughter nucleus produced by the coincident emission of a neutron and a proton,

$$\sigma^{A-2,Z-1}(U) = \frac{C_{np}}{2\sigma_{np}} \left[\frac{d\sigma_n(\epsilon)}{d\epsilon} \right] + \frac{C_{np}}{2\sigma_{pn}} \left[\frac{d\sigma_p(\epsilon)}{d\epsilon} \right], \quad (20)$$

where

$$U = E - B_n - B_p - \epsilon - \bar{\epsilon}_{p(n)}$$

as previously defined, and where $\bar{\epsilon}_{p(n)}$ is the average kinetic energy of the proton (neutron) emitted in coincidence with a neutron (proton) of kinetic energy ϵ . An expression analogous to Eq. (19) is used for the case of two proton

emission.

We state again that these procedures are crude and arbitrary. We feel that they should provide a first order correction to the previous neglect of multiple precompound decay, and we can readily understand that a more sophisticated treatment which includes type II decay should yield higher multiple precompound decay fractions.

Several previous investigations have addressed the question of multiple precompound decay.^{38–40} The equivalent of our Eq. (1) in those works is normalized to the number of nuclei in the ensemble rather than to the number of particles. It then follows that the parent nucleus decay populates a daughter product characterized by one exciton number less, at an appropriate residual excitation energy. The daughter ensemble is then treated again by the equivalent of Eq. (1), etc. This seems a more natural manner of simultaneously treating our type I and type II decays, without the necessity of invoking the algorithms in Eqs. (12)–(20) of this work. However, it raises a normalization question which we feel needs resolution before we attempt to implement this approach within the hybrid model formulation.

The algorithms presented limit multiple precompound decay to two particle emission. For nucleon induced reactions at energies below 200 MeV considered in this work, we think that this does not provide a serious shortcoming. The types of algorithms employed could be extended beyond the two particle limit if necessary.

We have made comparisons for the reactions $^{202}\text{Hg}(p,2p)$ and $^{202}\text{Hg}(p,2pn)$ using the new multiple emission algorithms versus the older single precompound particle emission decay code.⁴¹ These excitation functions should provide a fairly rigorous test of the multiple decay assumptions, as proton evaporation is very highly inhibit-

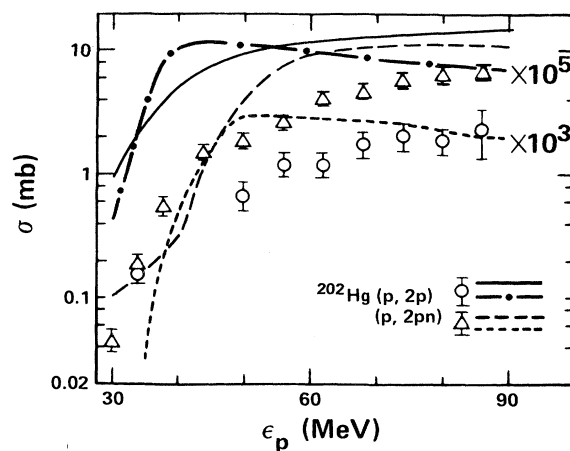


FIG. 9. Calculated and experimental $^{202}\text{Hg}(p,2p)$ and $(p,2pn)$ excitation functions. The points represent experimental yields from Ref. 41. The long dashed curve is the $(p,2pn)$ prediction of this work, and the solid line the $(p,2p)$ result. Multiple precompound decay algorithms are used in these results. The dotted-dashed curve is the GDH result ($\times 10^5$) for $(p,2p)$ from the precompound formulation without multiple precompound decay, and the short dashed curve is the same ($\times 10^3$) for the $(p,2pn)$ reaction.

ed in nuclei of high atomic numbers. The proton emission yields should therefore result primarily from the precompound process. Comparisons are shown in Fig. 9. The earlier GDH-evaporation calculation²¹ may be seen to give poor shapes for the excitation functions, and more significantly to underestimate yields of the (p,2pn) and (p,2p) products by 3 and 5 orders of magnitude, respectively. The new algorithm gives cross sections to the correct order of magnitude, and quite satisfactory shapes over nearly the entire energy range. It should be emphasized that these cross sections are only around 0.3% of the reaction cross section, so that the fraction of the reaction cross section calculated to populate these yields is given surprisingly well. However, many more such comparisons must be made before becoming comfortable with this observation.

8. Evaporation calculation level densities

The Fermi gas level density used²² is of the form

$$p(U) \propto (U - \delta)^{-5/4} \exp 2\sqrt{a(U - \delta)}, \quad (21)$$

where the pairing options were described in Sec. II B 4. The level density parameter "a" was evaluated as $A/9$, which is the default option of the code.²² Level density and pairing values might better be selected from experimental results for a given target nucleus, when available. However, we describe a global treatment in this work, rather than attempts at best fits in narrow mass regions.

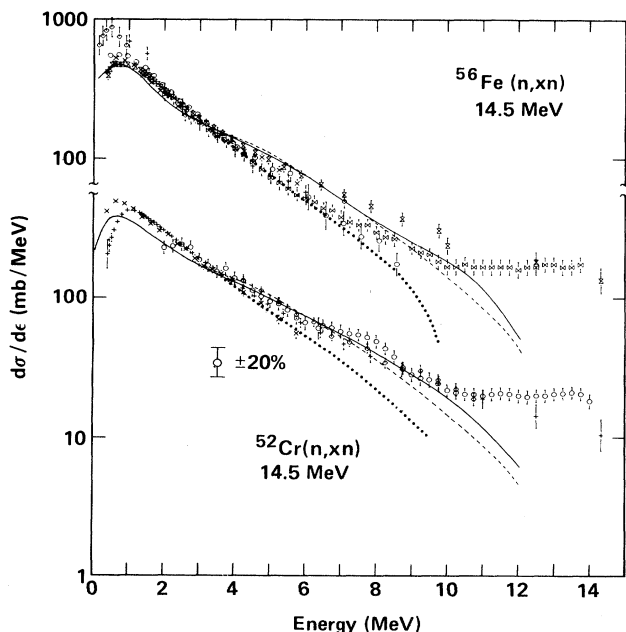


FIG. 10. Calculated and experimental (n,xn) spectra for 14.5 MeV neutrons on ^{52}Cr and ^{56}Fe targets. Calculations were performed for ^{52}Cr and ^{56}Fe . The solid line represents evaporation plus GDH; the dashed line is the evaporation plus hybrid result. The dotted lines are pure evaporation. The experimental yields are from Refs. 42–48.

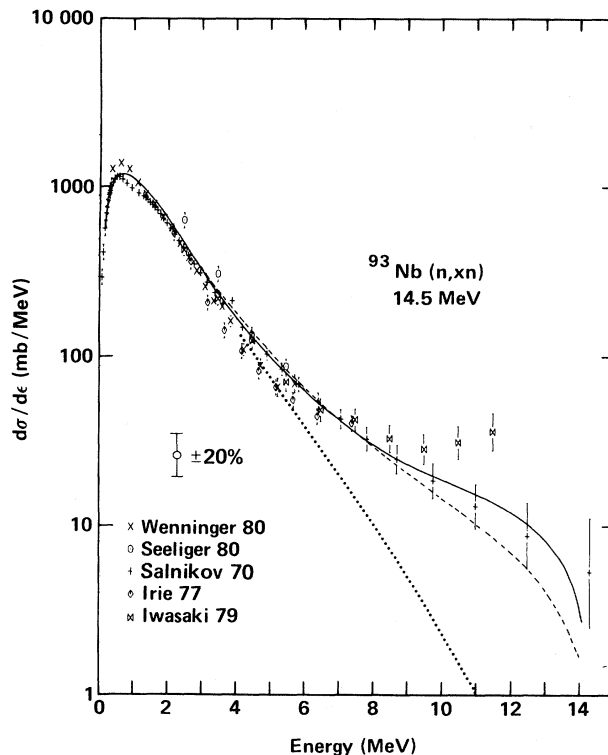


FIG. 11. As in Fig. 10 for $^{93}\text{Nb} + 14.5$ MeV neutrons. Experimental results are from Refs. 42, 44, 49, and 50.

III. COMPARISONS OF EXPERIMENTAL AND CALCULATED NUCLEON SPECTRA

Calculated and experimental particle spectra are compared for (n,xn) reactions in Figs. 10 and 11, for (n,p) reactions in Fig. 12, for (p,n) reactions in Figs. 13–20, and for (p,p') reactions in Figs. 19–22. In the following subsections, these comparisons are discussed first in the category of neutron induced reactions, and second of proton induced reactions.

A. Neutron induced reactions

The data presented in Figs. 10–12 are all for incident neutrons of 14.6 ± 0.6 MeV.^{42–52} There is a paucity of data for higher neutron energies, although some (n,p) measurements with 26 and 60 MeV neutrons have recently been completed.^{53,54}

For the 14.5 MeV incident neutron energy range it is difficult to assess the success of the precompound calculation below $A = 80$, since compound yields are comparable to measured differential cross sections. The precompound calculation may then yield a small component relative to the equilibrium yield, so that small uncertainties in the latter cause very large uncertainties in the validity of the predicted precompound component. This is clear in Fig. 10, where it may be seen that small temperature changes in the evaporation spectra would have a large effect on the amount of precompound decay necessary to reproduce the experimental results. However, for the ^{93}Nb target (Fig.

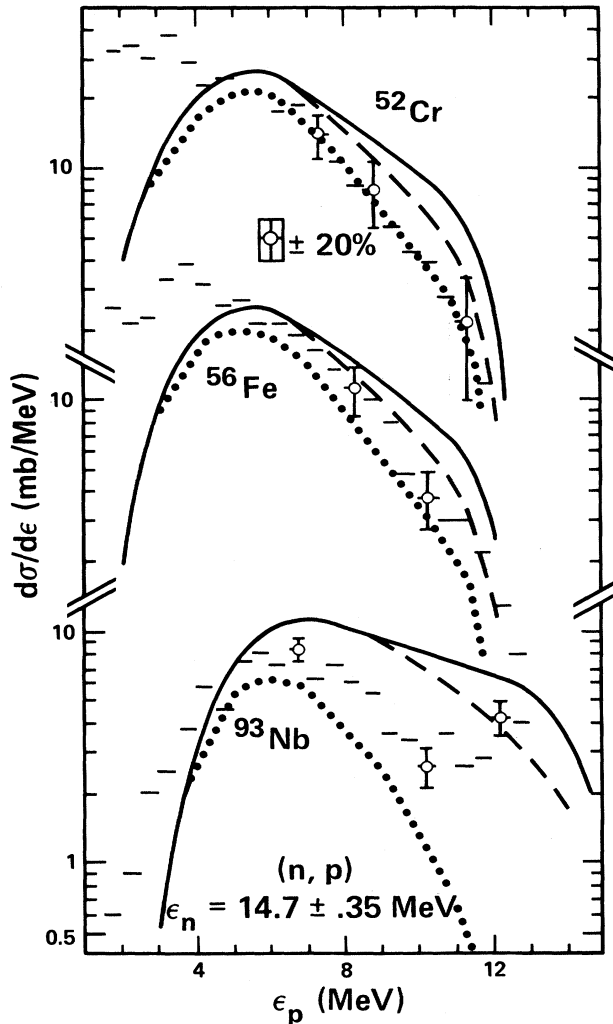


FIG. 12. Calculated and experimental results for (n,p) spectra on ^{52}Cr , ^{56}Fe , and ^{93}Nb with 14.7 ± 0.35 MeV neutrons. The solid curves represent evaporation plus GDH predictions, the dashed lines evaporation plus hybrid model, and the dotted lines pure evaporation predictions. Representative error bars have been placed on a few of the experimental cross sections. Experimental yields are from Refs. 51 and 52.

11) the compound evaporation component is soft enough versus the experimental spectra (above 9 MeV) that one can test the precompound models. This is due just to the compound nucleus temperature dependence on mass number ($T = \sqrt{kE/A}$).

For the example in Fig. 11, the hybrid and GDH models both adequately describe the experimental results. The difference between these approaches is within the $\pm 20\%$ "noise" level over most of the energy range.

The (n,p) spectra are shown in Fig. 12. Here the compound spectra for ^{52}Cr and ^{56}Fe targets can again greatly change the precompound contributions necessary to fit the experimental spectra. This is not the case for ^{93}Nb . For the latter case the (n,p) precompound spectra are too high over a part of the high energy range. The main conclusion, however, is that higher neutron energies are really

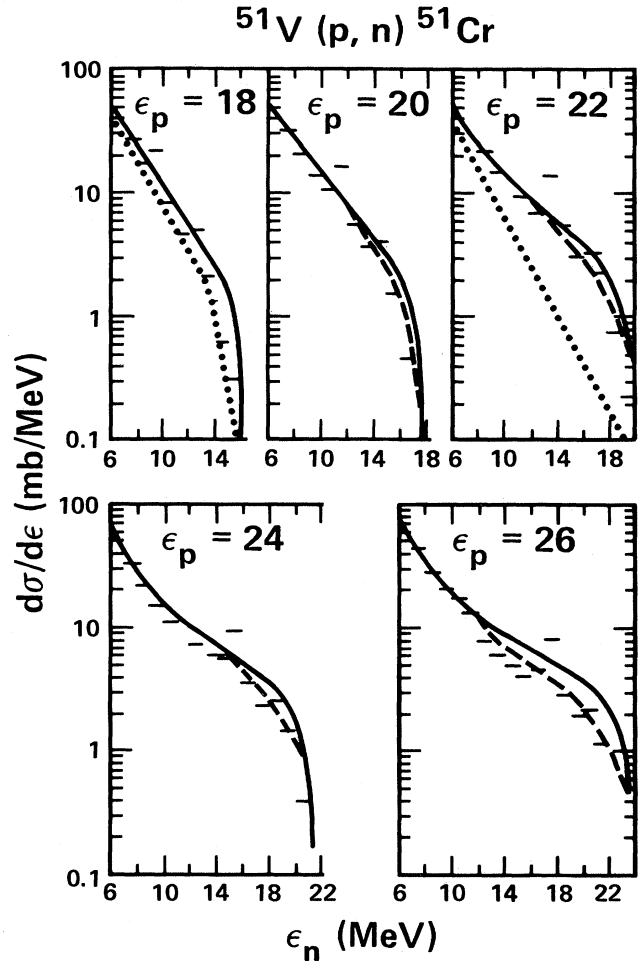


FIG. 13. Experimental and calculated neutron spectra for the reaction $^{51}\text{V}(p,n)^{51}\text{Cr}$ at proton energies between 19 and 26 MeV. The calculated curves are as in Fig. 12. Data given by bars are from Ref. 55.

necessary to test the (n,p) predictions. Comparisons of $^{58}\text{Ni}(n,p)$ results at 60 MeV neutron energy show excellent agreement between the GDH and experimental particle spectra.⁵⁴ The question of the overestimation of calculated $^{93}\text{Nb}(n,p)$ yields in Fig. 12 remains open. However, based on the Davis results,⁵⁴ we believe that the overestimation shown in Fig. 12 is not representative of the model in fitting (n,p) spectra, but rather is peculiar to fitting in the near barrier region.

For obvious experimental reasons there is a far broader body of proton induced reaction data than of neutron induced reaction data. Comparisons of calculated and experimental (p,n) spectra are shown in Figs. 13–20,^{30,55–57} and of (p,p') spectra in Figs. 19–22.^{58,59}

The $^{51}\text{V}(p,n)$ data in Fig. 13 are reproduced quite well by the hybrid model; the GDH and hybrid models give quite similar spectra up to $\epsilon_p = 22$ MeV. At the higher energies the GDH result is too hard for neutron energies beyond 14 MeV. The odd-even pairing treatment option used reproduces the spectral end points quite well.

Some of the extensive (p,n) spectra reported by Grimes

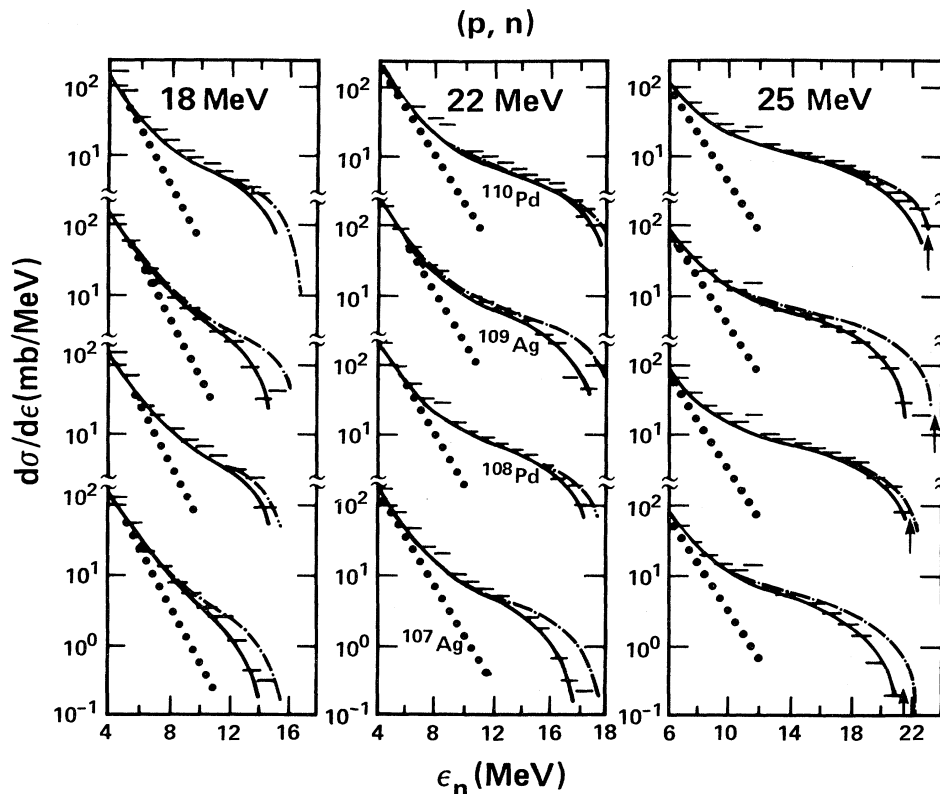


FIG. 14. As in Fig. 13 for (p,n) reactions on $^{107,109}\text{Ag}$ and $^{108,110}\text{Pd}$ targets. The dotted curve is the pure evaporation component of the calculated result. The solid curves are evaporation + GDH model results of Ref. 30. The dotted-dashed curve is the result of evaporation + GDH of this work using the odd-even reference surface pairing option, as discussed in the text. Data given by bars are from Ref. 30. Note that two sets of GDH calculations are compared in this figure, while Fig. 13 compares hybrid with GDH model results.

et al. in the mass 103–110 region³⁰ are compared with GDH calculations in Fig. 14. For all the results shown the hybrid and GDH results are practically identical, contrary to the results of Fig. 13. This is related to the alignment of the partial reaction cross sections from the optical model with the assumed matter density distribution based on Eqs. (4), (6), and (7), as illustrated in part in Figs. 1 and 2. The optical model routine puts a somewhat higher reaction cross section at lower densities for the lighter targets. The GDH results are reasonably sensitive to this alignment as the $^{51}\text{V}(p,n)$ spectra would indicate. This is also one of several reasons for the overestimation of the (n,p) spectra for 14 MeV incident neutrons.

The calculated (p,n) spectra in Fig. 14 agree well for all targets over the major portion of the compound and precompound spectra. They agree only with the ^{110}Pd and ^{108}Pd (and $^{106,104}\text{Pd}$ of Ref. 30 not shown here) over the entire energy range. These data support the suggestion of Grimes *et al.* that the precompound pairing treatment should be based on the particle-hole pairs created in the initial projectile-target interaction as discussed in (30) and summarized in Sec. II B 4. The excellent agreement of the GDH calculation of Ref. 30 when such a pairing option is used may be seen in Fig. 14, where Grimes's results are reproduced. The code used in this work gives the same results when the same pairing option is used.

There seems, however, to be some inconsistency between the agreement for $^{51}\text{V}(p,n)$ and disagreement for $^{107,109}\text{Ag}(p,n)$ between calculated and experimental spectra, when the pairing is treated using an odd-even reference surface as described in Sec. II B 4. Similarly, experimental

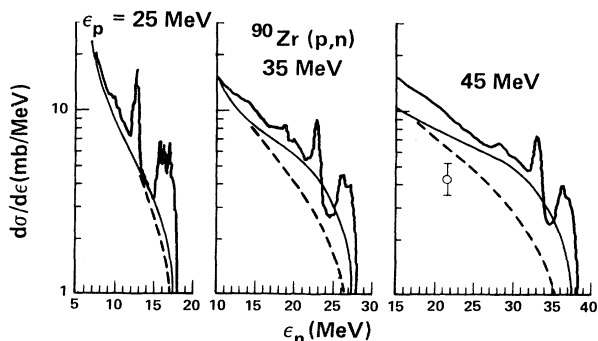
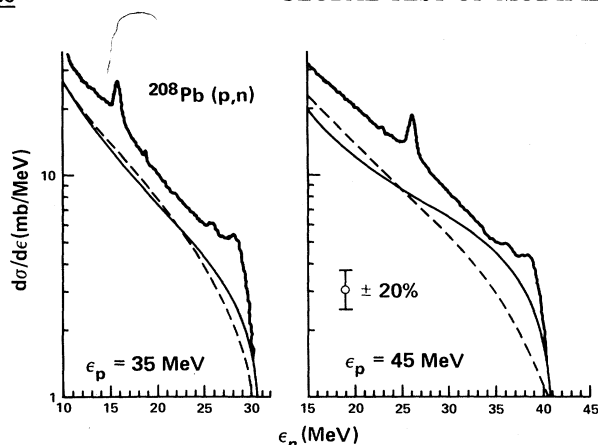
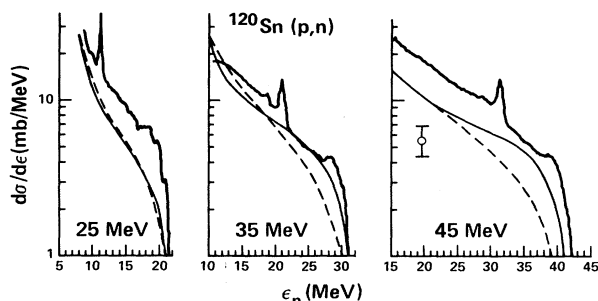
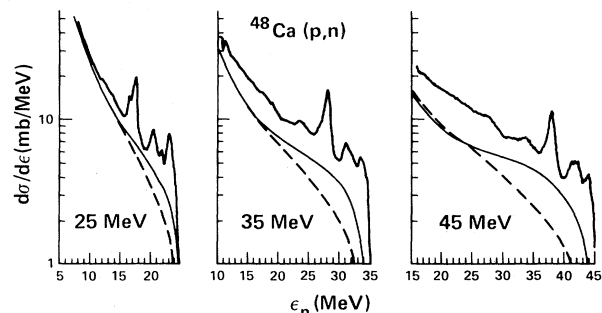


FIG. 15. Calculated and experimental (p,n) spectra on ^{90}Zr targets for 25, 35, and 45 MeV proton energies. The point with error bar represents a $\pm 20\%$ uncertainty characteristic of the noise level of the calculations. The thin solid curve is GDH + evaporation; the dashed curve is the hybrid model + evaporation result. The experimental spectra are from Ref. 56.

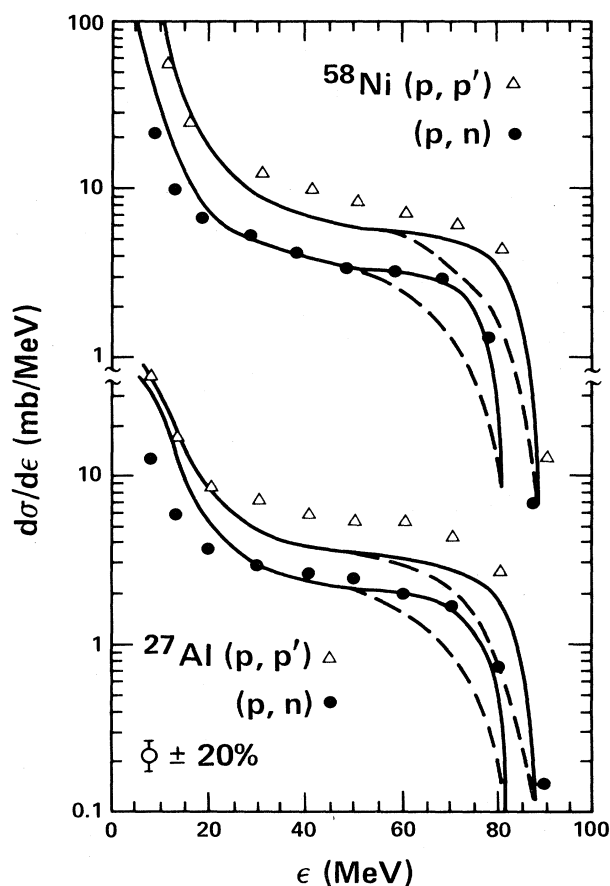
FIG. 16. As in Fig. 15 for a ^{208}Pb target.

end points for ^{64}Zn , ^{65}Cu , and $^{89}\text{Y}(p,n)$ spectra (26 MeV incident protons) are not reproduced at all well when the conventions of Ref. 30 are adopted.⁶⁰ In view of these observations, it would seem that the question of how to treat pairing in precompound decay is not yet unambiguously answered. The results of Figs. 13 and 14 may well be due to a combination of pairing and shell effects, whereby a single shift parameter is inadequate to describe both. It would be worthwhile to perform the careful and extensive type of measurements of Grimes *et al.*, in other mass regions, and also to seek clues from microscopic few-quasi particle exciton state density models in the interpretation of such results.^{61,62}

The pairing question becomes less important as bombarding energies increase. Results of (p,n) measurements at energies between 25 and 90 MeV are shown in Figs. 15–20. The GDH calculation reproduces all these (p,n) spectra quite well, for the most part to within the 20–30% noise level of calculational uncertainty. For the ^{208}Pb , ^{209}Bi , ^{90}Zr , ^{120}Sn , and ^{48}Ca targets the shape of the spectrum predicted by the hybrid calculation is in better agreement with experiment than the GDH result. For the ^{208}Pb and ^{209}Bi targets the hybrid model cross sections are too low by $\approx 35\%$ as they are for $^{90}\text{Zr}(p,n)$ at 45 MeV. For ^{120}Sn and ^{48}Ca they are too low by $\approx 50\%$. The GDH calculation reproduces both the magnitude and shapes of the (p,n) spectra on ^{27}Al and ^{58}Ni targets (Fig. 18) whereas the hybrid result does very poorly for the highest 30 MeV of neutron energy.

FIG. 17. As in Fig. 15 for a ^{120}Sn target.FIG. 18. As in Fig. 15 for a ^{48}Ca target.

Spectra for (p,p') reactions are shown in Figs. 19–22. The GDH calculation reproduces the precompound portion of these spectra extremely well versus the $\approx 20\%$ noise criterion. There is some overestimation of yields in the evaporation region, which calls attention again to the question of inverse reaction cross sections in the near barrier region. In Fig. 22, we have extended the GDH precompound calculation (without evaporation component) to emphasize that the (slight) failure of the calcu-

FIG. 19. Calculated and experimental $^{27}\text{Al}(p,p')$, (p,n) and $^{58}\text{Ni}(p,p')$, (p,n) spectra for 90 MeV incident protons. Experimental results are from Refs. 57 and 58. Calculated results are as in Fig. 15.

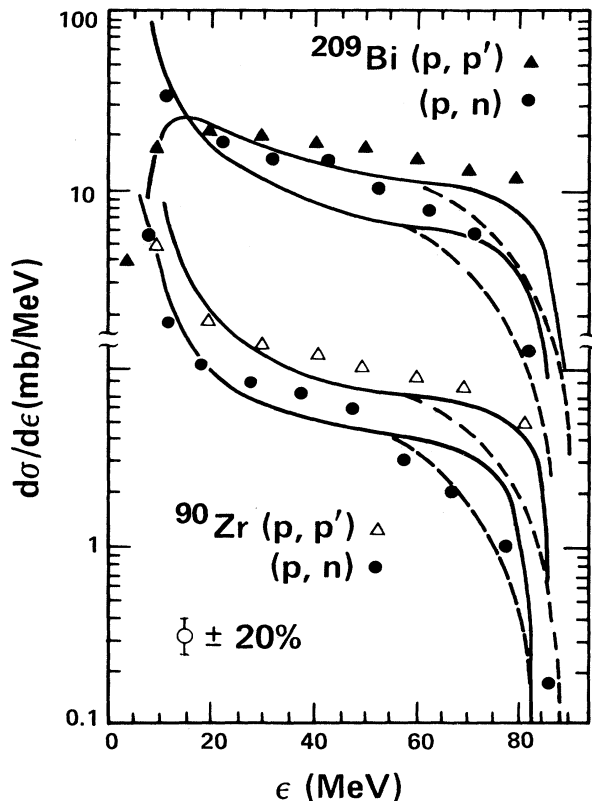


FIG. 20. As in Fig. 19 for ^{209}Bi and ^{90}Zr targets.

lation at lower energies is mainly an equilibrium problem. In the $^{209}\text{Bi}(p,p')$ spectrum the problem also shows up in the low energy precompound spectrum.

Hybrid model results for the (p,p') spectra are also shown in Figs. 19–22. In contrast to some of the (p,n) results, the calculated spectra are all in very much poorer agreement with experimental results than GDH model spectra. The (p,p') spectra all seem to be reproduced well

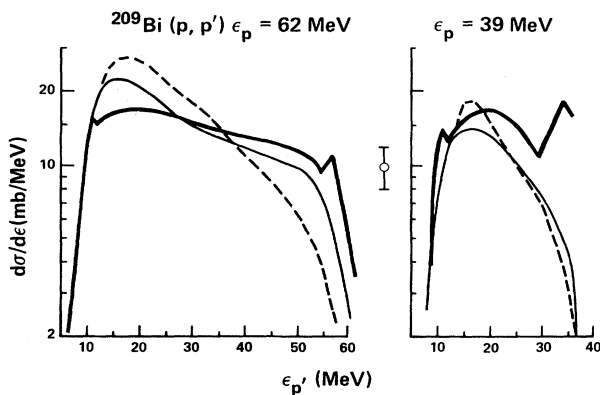


FIG. 21. Calculated and experimental spectra for $^{209}\text{Bi}(p,p')$ at proton energies of 39 and 62 MeV. The experimental angle integrated spectrum is given by the heavy solid curve, representing results from Ref. 59. Calculated results are as in Fig. 15.

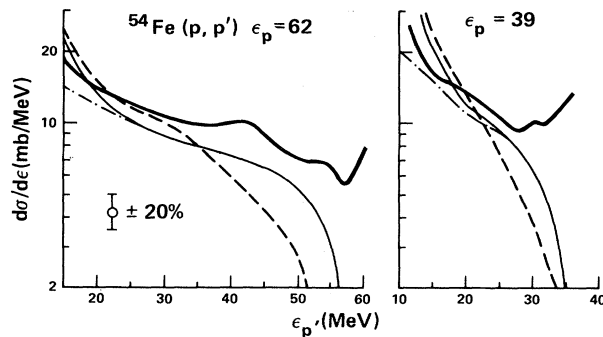


FIG. 22. Calculated and experimental spectra for $^{54}\text{Fe}(p,p')$ at 39 and 62 MeV proton energy. As in Fig. 21, experimental results are from Ref. 59. The dotted-dashed extension of the GDH + evaporation curve is the pure GDH contribution (no evaporation).

by the GDH model, and they are poorly reproduced by the hybrid model. The (p,n) spectra are reproduced reasonably well by the GDH model; however, targets with high neutron excesses decrease more rapidly at the highest kinetic energies than predicted by GDH. For the latter nuclei the hybrid model predicts better spectral shapes; the magnitudes of the hybrid model results on these neutron rich nuclei are low for most of the data. Whether these differences may be attributed to the neutron rich nature of the target nuclei is an open and provocative question. Isospin and/or the neutron skin may well be involved. It would be valuable to have (p,n) data in the 45 MeV (or higher) proton energy range on targets for which isospin and neutron skins varied, e.g., ^{40}Ca and ^{48}Ca , ^{58}Ni and ^{64}Ni , ^{92}Mo and ^{100}Mo , and also for a few targets with high isospin and large neutron excess, but away from shell closures, e.g., ^{149}Tb .

The latter suggestions deal with possible target properties which might be involved in the discrepancies between calculated and experimental precompound spectra. There are also considerations to be applied to the models in seeking to understand those differences which are apparently beyond the noise level.

One assumption worthy of further investigation is the use of a hole depth limited exciton distribution function, $N_n(E)$, only for the first collision. Higher exciton number energy partitions may be important only over a limited nuclear density range, so that expressions for $N_n(E)$ with limited hole depth should be tried. This should increase the medium energy emission components at the higher bombarding energies of Figs. 15–22, thus improving simultaneously the shape and magnitude of the (p,n) spectra. The (p,p') spectra could also improve in such a calculation.

Effects of isospin should be incorporated into the precompound decay model. This is in progress but results are not yet available. Microscopic exciton partition functions^{61,62,30} should similarly be investigated further to see the degree to which shell effects might perturb the particle spectra versus the equidistant model result for $N_n(E)$. It may also be necessary to consider explicitly multiple

precompound decay of type II, which would also increase spectral yields in the medium energy region, as is generally needed to improve the quality of fit to the higher energy data.

IV. CONCLUSIONS

A broad range of comparisons has been presented between experimental (N,N') spectra (where N =nucleon) and predictions of the hybrid and GDH models. The models have been modified with respect to earlier formulations in order to include the more important one of two possible modes of precompound decay in which more than one precompound particle may be emitted by a single nucleus. Additionally, the GDH density distribution was modified in an *ad hoc* manner, incorporating results of the droplet model.²⁵ A single consistent set of parameters from available options was adopted for testing the entire data set presented in this work, and this is described in Sec. II and in the references cited therein.

The results of these comparisons may be summarized according to overall success of the models on the one hand, and significant shortcomings on the other. In the first category, the multiple precompound decay algorithm resulted in predicted $(p,2p)$ and $(p,2pn)$ cross sections in fair agreement with experimental yields, even though these were only of the order of 0.3% of the reaction cross section. Earlier versions of the GDH model gave errors of 10^3 – 10^5 in these yields, strongly supporting the conclusion that they result from a multiple precompound decay mechanism. This new algorithm also leads to satisfactory yields for the (p,p') and (p,n) spectra at 90 MeV, which are superior to results of the earlier formulation.

The GDH formulation generally gives satisfactory agreement in absolute differential cross sections to within the $\pm 20\%$ noise level for the (n,n') , (p,n) , and (p,p') reactions spanning targets from ^{27}Al to ^{209}Bi , and incident particle energies between 14 and 90 MeV. The degree of success over a very wide dynamic range is really quite impressive for the simple models being used. There are some shortcomings for the $^{51}\text{V}(p,n)$ data at 24 and 26 MeV which we attribute to partial reaction cross section versus density profile mismatch rather than a failure in the model *per se*. The last few MeV of the precompound spectra in the mass 104–110 region are sensitive to the manner in which pairing is entered into the precompound calculation. We believe that this remains an open question, and suspect that the gap parameters may need a shell component as well as a pairing component. Yields of some (p,n) reactions at 90 MeV proton energy are overestimated at higher neutron energies by the GDH model.

Many of the calculated (p,n) and (p,p') spectra at the higher bombarding energies are somewhat too low in absolute magnitude. Future improvement may result from use of exciton energy partition functions derived for a limited hole depth and an effective Fermi energy characteristic of some portion of the surface responsible for precompound decay. The inclusion of multiple precompound decay of type II (see Sec. II) will also reduce the discrepancy in the medium energy region, though only by 10–20%.

Some comparisons between calculated and experimental

(p,n) spectra suggest the desirability of additional experimental results to assess possible influences of shell effects and of effects due to neutron excess on the observed particle spectra. When experimental results as suggested become available, and when some of the microscopic $N_n(E)$ results are investigated in greater depth, we may then see whether the models are capable of still better predictive powers with better input, or whether instead we are asking to reproduce details which are beyond the physical content of even improved formulations of the models.

APPENDIX

The exciton model decay formulations are governed by what have been called exciton state densities $[\rho_n(E)]$ or scattering distribution functions $[N_n(E)]$ in much the same manner as the level density influences the evaporation spectrum. It is important to understand the source of these functions, and the nature of inherent errors in them in order to understand limits of accuracy which might possibly be expected between calculated and experimental results, if the models themselves were otherwise correct.

The usual exciton distribution functions derived in the context of Fermi gas models have been discussed previously^{18,23}; however, the literature sources are not readily available to many readers, so a part of the discussion is repeated here for completeness.

There is first a neglect of Pauli exclusion in the population of excited levels. However, correction functions have been derived for this effect, beginning with the work of Williams.⁶³ It has also been demonstrated that this is a rather negligible effect in the precompound region,¹⁸ although the correction factors⁶³ are included in the ALICE/LIVERMORE 82 and ALICE precompound routines.

We wish to address the question of the validity of the exciton distribution function $[\rho_n(E)$ or $N_n(E)]$ as giving the population versus excitation which would result from multiple two-body scattering following the kinematics of free nucleon-nucleon scattering, modified by the Pauli exclusion principle. This dynamic justification of the distribution function is necessary since the relative scattering rates expected within a given exciton hierarchy are very much less than those resulting in creation of a p-h pair. With this in mind we reproduce below a derivation of the distribution function based on the dynamics of nucleon-nucleon scattering.²³ We begin with a hypothesis, derive the distribution function, and then check the degree of accuracy of the hypothesis.

Hypothesis: For the process of nucleon-nucleon scattering in nuclear matter as initiated by an incident nucleon, the differential cross section $d\sigma/d\epsilon$ for all final energies is constant independent of the nucleon energy of the partner to be scattered.

Let us consider a nucleon entering a nuclear well, as shown in Fig. 23. The particle can scatter with nucleons having an energy within one unit of the Fermi energy, giving a $2p1h$ distribution. There are E' equally likely ways this can be done where $E'=gE$, and $1/g$ is the natural unit of energy. The “equally likely” statement is a consequence of the kinematic hypothesis made above.

The particle could also scatter with nucleons having en-

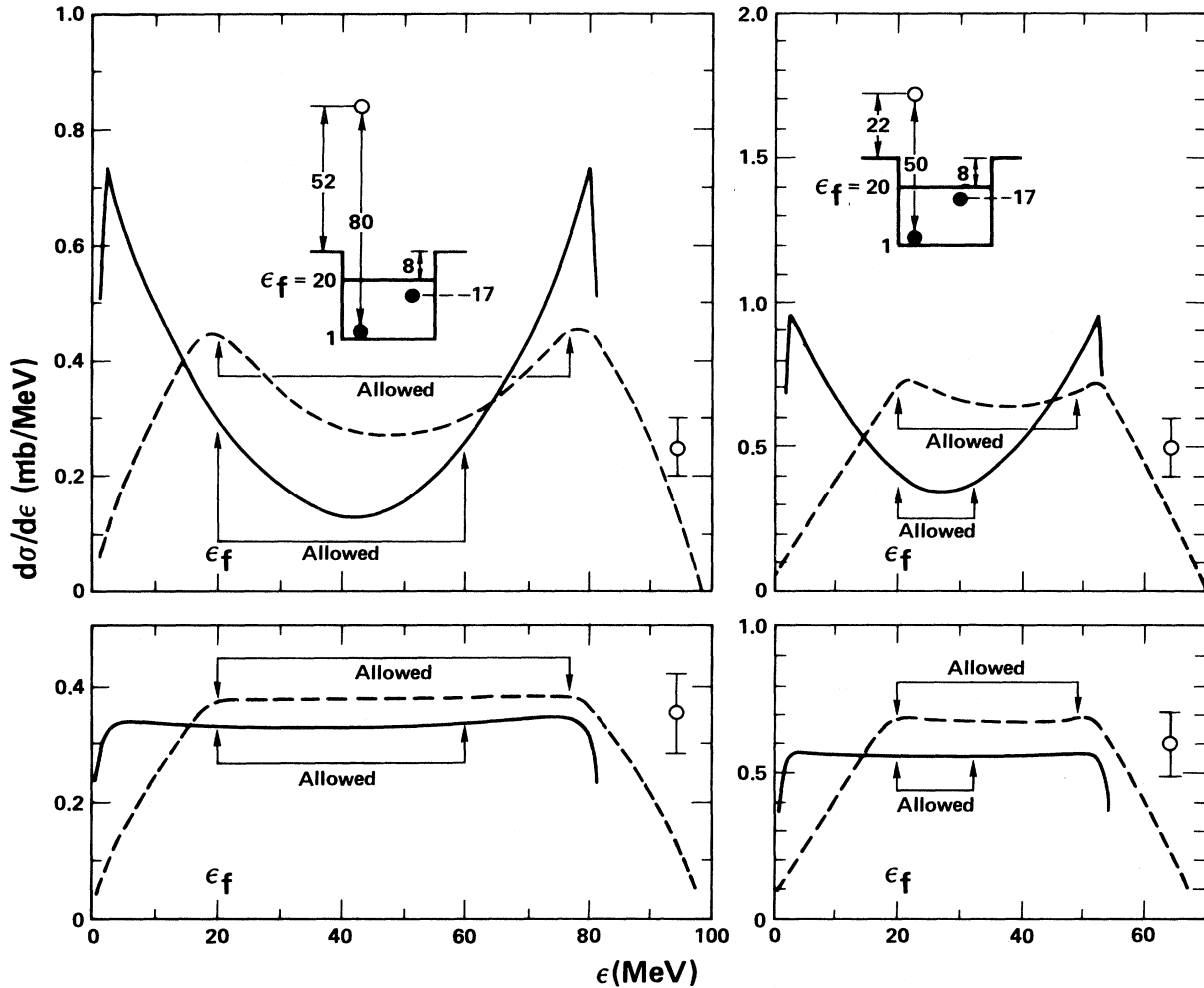


FIG. 23. Angle averaged spectra for nucleon-nucleon scattering. Spectra are averaged over all initial and final scattering angles using anisotropic free scattering angular distributions (upper figures) or isotropic free scattering angular distributions (lower curves). Particle 1 energies of 1 and 17 MeV are shown versus particle 2 energies of 50 and 80 MeV relative to the well bottoms. The upper and lower Pauli exclusion cutoffs are indicated for scattering within a nucleus for which the Fermi energy is 20 MeV. The small drawings above each set of differential cross sections represents the energy relationships of the two nucleons and the nuclear potential.

ergies between one and two units below E_f ; there would be $E' - 1$ equally likely ways this could happen rather than E' ways, since one possibility is now excluded by the Pauli principle. And it may be seen that the total number of allowed arrangements due to scattering with the hypothesis above is given by

$$N_{2p1h}(E) = \frac{1}{2!} \int_0^{E'} (E' - x) dx = \frac{g^2 E^2}{2!2!}, \quad (\text{A1})$$

where the $2!$ is added before the integral to correct for multiple counting of the two indistinguishable particles. The result of this argument can be extended to the general case of $n = p + h$ excitons,

$$N_n(E) = E^{n-1} / [p!h!(n-1)!], \quad (\text{A2})$$

and it is seen that this is identical to the Ericson formula⁶⁴ times a constant,

$$N_n(E) = \rho_n(E) / g. \quad (\text{A3})$$

And so, to the extent that the hypothesis made above is valid, it may be seen that the scattering distribution function $N_n(E)$, derived from considerations of the kinematically determined exciton energy scattering distributions, is identical to the Ericson result. But now we must see to what extent the hypothesis on which (A2) is based is valid.

Figure 23 shows results of a nucleon-nucleon scattering calculating for a nucleus with a Fermi energy of 20 MeV. The collisions were averaged over all incident scattering angles between the nucleons above and below the Fermi energy. Free scattering angular distributions were used as a library in these calculations. Additional details may be found elsewhere.^{65,66} Two "sets" of results are shown in Fig. 23. One is for an exciton of energy 50 MeV (relative to the bottom of the nuclear potential well) colliding with nucleons of 1 and 17 MeV within the nuclear potential. This means that one exciton is initially above E_f ; the other is below E_f . No Pauli correction is applied in calculating the $d\sigma/d\epsilon$ following the angle averaged collision of the

nucleon-nucleon pair. The second set of calculations is for one exciton initially at 80 MeV above the nuclear well bottom, with the same choices of energy for its collision partner as in the 50 MeV example. Calculations are shown for an isotropic N-N scattering angular distribution (nn or np scattering), and for an anisotropic distribution (p,p scattering).

The relevant scattering cross sections for both sets of results shown in Fig. 23 are in the energy range above E_f and below the initial exciton energy (50 or 80 MeV). This is simply the statement of the Pauli exclusion principle and energy conservation. Our hypothesis for the validity of Eq. (A2) is the equality of all $d\sigma/d\epsilon$ for a single initial exciton energy above E_f with all exciton energies below E_f . It is *not* required that the $d\sigma/d\epsilon$ for set 1 be equal to the $d\sigma/d\epsilon$ for set 2 for Eq. (A2) to be a valid result for a multiple scattering process. Such cross section variations show up as emission to spreading rate differences, not as

differences in population probabilities over the collisional cascade.

It may be seen in Fig. 23 that our required hypothesis is not precisely fulfilled. However, it is satisfied to well within a $\pm 20\%$ range for isotropic N-N angular distributions, and nearly to within this range for the anisotropic case. We, therefore, should not expect the precompound formulas based on Eq. (A2) to be any more reliable. To this uncertainty one should fold in a $\pm 10\text{--}20\%$ uncertainty in the inverse reaction cross sections entering precompound decay models, resulting in a calculational noise level of at least 20–30%.

This work was performed under the auspices of the U. S. Department of Energy by the Lawrence Livermore National Laboratory under Contract No. W-7405-ENG-48.

*Permanent address: Institut für Radium forschung und Kernphysik, Boltzmannngasse 3, Vienna, Austria.

- ¹J. J. Griffin, Phys. Rev. Lett. **17**, 478 (1966).
- ²J. J. Griffin, in *Intermediate Structure in Nuclear Reactions*, edited by H. P. Kennedy and R. Schriels (University of Kentucky Press, Lexington, 1968).
- ³J. J. Griffin, in *Nuclear Physics: An International Conference*, edited by L. Becker, C. D. Goodman, P. H. Stelson, and A. Zucker (Academic, New York, 1967), p. 778.
- ⁴J. J. Griffin, Phys. Lett. **24B**, 5 (1967).
- ⁵G. D. Harp and J. M. Miller, Phys. Rev. C **3**, 1847 (1971).
- ⁶M. Blann, Phys. Rev. Lett. **27**, 337 (1971); **27**, 700(E) (1971); **27**, 1550(E) (1971).
- ⁷M. Blann, Phys. Rev. Lett. **28**, 757 (1972).
- ⁸M. Blann and A. Mignerey, Nucl. Phys. **A186**, 245 (1972).
- ⁹M. Blann, Nucl. Phys. **A213**, 570 (1973).
- ¹⁰F. Gadioli, E. Gadioli-Erba, and P. G. Sona, Nucl. Phys. **A217**, 589 (1973).
- ¹¹C. Birattari *et al.*, Nucl. Phys. **A166**, 605 (1971).
- ¹²C. Birattari *et al.*, Nucl. Phys. **A166**, 605 (1973).
- ¹³C. Birattari, E. Gadioli, A. M. Grassi Strini, G. Strini, and G. Tagliaferri, Lett. Nuovo Cimento **7**, 101 (1973).
- ¹⁴E. Gadioli, A. M. Grassi Strini, G. LoBianco, G. Strini, and G. Tagliaferri, Nuovo Cimento **22**, 547 (1974).
- ¹⁵G. M. Braga-Marcazzan, E. Gadioli-Erba, L. Milazzo-Colli, and P. G. Sona, Phys. Rev. C **6**, 1398 (1972).
- ¹⁶E. Gadioli and L. Milazzo-Colli, in *Proceedings of the Europhysics Study Conference on Intermediate Processes in Nuclear Reactions, Yugoslavia, 1973*, edited by N. Cindro, P. Kulisic, and T. Mayer-Kuckuk (Springer, Heidelberg, 1973).
- ¹⁷E. Gadioli and E. Gadioli-Erba, Acta Phys. Slovaca **25**, 126 (1975).
- ¹⁸M. Blann, in *Proceedings of the Summer School of Nuclear Physics, 1974, Predeal, Romania*, edited by A. Ciocanel (Editura Academiei Republicii Socialiste Romania, Bucharest, 1976), p. 249.
- ¹⁹M. Blann, Annu. Rev. Nucl. Sci. **25**, 123 (1975).
- ²⁰M. Blann and F. Plasil, University of Rochester Report No. COO-3494-10, 1973 (unpublished).
- ²¹M. Blann, University of Rochester Report No. COO-3494-29, 1975 (unpublished).
- ²²M. Blann and J. Bisplinghoff, Lawrence Livermore National Laboratory Report No. UCID 19614, 1983 (unpublished).
- ²³M. Blann, A. Mignerey, and W. Scobel, Nukleonika **21**, 335 (1976).
- ²⁴R. Hofstadter, Annu. Rev. Nucl. Sci. **7**, 295 (1957).
- ²⁵R. D. Myers, *Droplet Model of Atomic Nuclei* (Plenum, New York, 1977).
- ²⁶A. Chevarier, N. Chevarier, A. Demeyer, G. Hollinger, P. Pertosa, and T. M. Duc, Phys. Rev. C **8**, 2155 (1973).
- ²⁷F. D. Becchetti and G. W. Greenlees, Phys. Rev. **182**, 1190 (1969).
- ²⁸K. Kikuchi and M. Kawai, *Nuclear Matter and Nuclear Interactions* (North-Holland, Amsterdam, 1968).
- ²⁹P. Schwandt *et al.*, Phys. Rev. C **23**, 1023 (1981).
- ³⁰S. M. Grimes, J. D. Anderson, and C. Wong, Phys. Rev. C **13**, 2224 (1976).
- ³¹J. R. Huizenga, H. K. Vonach, A. A. Katsanos, A. S. Gorski, and C. J. Stephan, Phys. Rev. **182**, 1149 (1969).
- ³²A. H. Wapstra and N. B. Gove, Nucl. Data Tables **9**, 265 (1971).
- ³³F. G. Perey, Phys. Rev. **131**, 745 (1963), and references therein to experimental proton reaction cross sections. See also J. J. H. Menet, E. E. Gross, J. J. Malanify, and A. Zucker, Phys. Rev. C **4**, 1114 (1971).
- ³⁴D. Wilmore and P. E. Hodgson, Nucl. Phys. **55**, 673 (1964).
- ³⁵Brookhaven National Laboratory Report No. BNL-325, 1966 (unpublished), and references to experimental data therein.
- ³⁶Brookhaven National Laboratory Report No. BNL-325, 1976 (unpublished), 3rd ed., No. VII, and references to experimental data therein.
- ³⁷M. Blann, Report No. UCRL-88757, 1983; Phys. Rev. C **28**, 1648 (1983).
- ³⁸K. Seidel, D. Seeliger, and A. Meister, Yad. Fiz. **23**, 745 (1976) [Sov. J. Nucl. Phys. **23**, 392 (1976)].
- ³⁹K. S. Ol'khovskii and V. A. Plyñiko, Yad. Fiz. **25**, 520 (1977) [Sov. J. Nucl. Phys. **25**, 279 (1979)].
- ⁴⁰J. M. Akkermans and H. Gruppelaar, Z. Phys. A **300**, 345 (1981).
- ⁴¹M. V. Kantelo and J. J. Hogan, Phys. Rev. C **13**, 1095 (1976).
- ⁴²O. A. Salnikov *et al.* Yad. Fiz. **12**, 1132 (1970) [Sov. J. Nucl. Phys. **122**, 620 (1971)].
- ⁴³D. Seeliger, private communication.
- ⁴⁴H. Vonach *et al.*, Brookhaven National Laboratory Report

- No. BNL-NCS 51245, 1980, p. 343.
- ⁴⁵G. Winkler, K. Hansjakob, and G. Stoffel, in the Proceedings of the International Conference on Nuclear Cross Sections for Technology, Knoxville, 1979, p. 150.
- ⁴⁶R. M. Schectmann *et al.*, Nucl. Phys. 77, 241 (1966).
- ⁴⁷G. Clayeux *et al.*, Commissariat A L'Energie Atomique Report No. 4279, 1972.
- ⁴⁸G. Stengl *et al.*, Nucl. Phys. A290, 109 (1977).
- ⁴⁹Y. Irie *et al.*, Mem. Fac. Eng. Kyushu Univ. 37, 19 (1977).
- ⁵⁰S. Iwasaki *et al.*, Ref. 45, p. 73.
- ⁵¹S. M. Grimes, R. C. Haight, and J. D. Anderson, Phys. Rev. C 17, 508 (1978).
- ⁵²S. M. Grimes, R. C. Haight, K. R. Alvar, H. H. Barschall, and R. R. Borchers, Phys. Rev. C 19, 2127 (1979).
- ⁵³R. Finlay (private communication).
- ⁵⁴C. Castaneda *et al.*, Phys. Rev. C 28, 1493 (1983).
- ⁵⁵S. M. Grimes, J. D. Anderson, J. C. Davis, and C. Wong, Phys. Rev. C 8, 1770 (1973).
- ⁵⁶M. Blann, R. R. Doering, A. Galonsky, D. M. Patterson, and F. E. Serr, Nucl. Phys. A257, 15 (1976).
- ⁵⁷A. M. Kalend *et al.*, Phys. Rev. C 28, 105 (1983).
- ⁵⁸J. R. Wu, C. C. Chang, and H. D. Holmgren, Phys. Rev. C 19, 698 (1979).
- ⁵⁹F. E. Bertrand and R. W. Peele, Phys. Rev. C 8, 1045 (1973).
- ⁶⁰W. Scobel, L. F. Hansen, B. A. Pohl, C. Wong, and M. Blann, Z. Phys. A 311, 323 (1983).
- ⁶¹F. C. Williams, Jr., A. Mignerey, and M. Blann, Nucl. Phys. A207, 619 (1973).
- ⁶²K. Albrecht and M. Blann, Phys. Rev. C 8, 1481 (1973).
- ⁶³F. C. Williams, Jr., Nucl. Phys. A166, 231 (1971).
- ⁶⁴T. Ericson, Adv. Phys. 9, 423 (1960).
- ⁶⁵A. Mignerey, M. Blann, and W. Scobel, Nucl. Phys. A273, 125 (1976).
- ⁶⁶W. Scobel, M. Blann, and A. Mignerey, Nucl. Phys. A287, 301 (1977).